Proceeding Series of the Brazilian Society of Computational and Applied Mathematics, v. 12, n. 1, 2026.

Trabalho apresentado no XLIV CNMAC, Fundação Getulio Vargas - Rio de Janeiro - RJ, 2025.

Proceeding Series of the Brazilian Society of Computational and Applied Mathematics

Investigation of a Conservative Finite Volume Scheme for Flows in Karstified Porous Media

Uebert G. Moreira[1], Fabricio S. Sousa[2]
ICMC-USP, São Carlos, SP
Franciane F. Rocha[3]
WIKKI Brasil, Rio de Janeiro, RJ

Abstract. Karstic geometries represent a distinct configuration characterized by the presence of conduits/channels (or vugs/chambers) intertwined within a porous medium. Modeling flow through such reservoirs poses a significant challenge, resulting in limited predictive capabilities regarding flow and transport processes. In this work, we formulate a finite-volume-mass conservative treatment for karst-matrix coupling. The designed scheme allows for handling complex geometrical karst configurations that contain volume cells significantly smaller than the underlying matrix, thereby increasing the applicability of the proposed model to the simulation of realistic karstified porous media problems. The investigated model is applied to different porous media configurations, with numerical results compared against reference solutions and verified by mass conservation evaluation.

Keywords. Porous Media, Conduits, Karst Index, Conservative Flow, Finite Volume Method.

1 Introduction

Numerical modeling of flows in karstified porous media is challenging due to the coupled dynamics between conduit and matrix flows, which are governed by different physical mechanisms. These challenges are exacerbated by the complex geometry of the conduit networks, the large differences in spatial scales, the pronounced heterogeneity, and the data uncertainties. Reservoirs differ in properties of their fluid systems, fractures, and cavity structures, thus exhibiting varied permeability characteristics and fluid flow patterns [11]. Notably, the heterogeneity stemming from conduit presence represents a crucial aspect to capture, as it can lead to varying degrees of resistance or facilitation to flow, depending on the flow direction [1]. Quantification and prediction of the hydromechanical behavior of these reservoirs pose significant challenges to the oil industry.

The modeling of karst also reaches its limits due to the lack of reliable geometric data and the high computational effort required for discretization. An alternative approach is to use more efficient models on coarser grids that can accurately reproduce the behavior of the original model. For example, characteristic parameters of the geometry can be homogenized to simplify the grid to one dimension. In addition, continuum formulations have been developed in which the mass transfer component is constitutively given in the form of an exchange coefficient whose reciprocal plays the rule of a conduction resistance multiplied by the pressure difference between the two substructures [4].

In this study, we formulate a finite volume mass conservative treatment to numerically characterize incompressible single-phase flows in karstified carbonate rocks within the embedded karst region, using a model that couples 3D/1D flow systems. Our approach incorporates the concept of

[1] uebert.moreira@usp.br
[2] fsimeoni@icmc.usp.br
[3] fr.franciane@alumni.usp.br

the Karst Index (K_I) introduced by [8], and its application follows a similar methodology to that of the Well Index outlined by [10] and further investigated by [1]. This framework offers several advantages, including the use of experiment-specific parameters and the generation of individualized coefficients for each cell, as opposed to applying a singular global value for each branch as we performed in [7]. We perform simulations focusing on a slab geometry problem in a domain $\Omega \subset \mathbb{R}^3$, taking into account the presence of karst conduits with high permeability contrast relative to the porous matrix.

The following section presents the mathematical and numerical formulations investigated in this work. Numerical experiments and discussions are presented in Section 3. Finally, concluding comments and suggestions for future work are made in Section 4.

2 Mathematical and Numerical Settings

The equations used in this study are consistent with those described in our previous publication [7] and other recent works [5, 8], where the studied region, Ω, is a subset of $\mathbb{R}^3$ that includes the conduit system, γ. The local hydrodynamics is determined by an elliptic system for porous matrix (m) coupled with transfer conditions to the conduit (c). We study the flow of a single-phase incompressible fluid in a carbonate matrix comprising a network of karst conduits, neglecting gravitational and inertial effects for simplicity. Our goal is to derive approximations for the coupled reduced model [3, 5, 8], finding the flux $\mathbf{u}_m(\mathbf{x})$ in the porous matrix, the average flux $u_c(s)$ within the karst conduit, and the pressures $p_m(\mathbf{x})$ and $p_c(s)$, satisfying:

$$\begin{cases} \nabla \cdot \mathbf{u}_m = \dfrac{K_I}{\mu}(p_c - p_m)\delta_{cm} + q\delta_m, & \text{in } \Omega, \\ \mathbf{u}_m = -\dfrac{K_m}{\mu}\nabla p_m, & \text{in } \Omega, \\ \dfrac{du_c}{ds} = -\dfrac{1}{A_c}\dfrac{K_I}{\mu}(p_c - p_m), & \text{in } \gamma, \\ u_c = -\dfrac{K_c}{\mu}\dfrac{dp_c}{ds}, & \text{in } \gamma. \end{cases} \tag{1}$$

Here, $\mathbf{x} \in \Omega$ denotes the spatial matrix position, $s \in \gamma$ is the coordinate along the conduit symmetry line, q a source term, K_I the karst index, μ the fluid viscosity, K_m and K_c the permeabilities of porous matrix and conduit, respectively. The δ correspond to Dirac function that impose line sources: δ_{cm} for interface between matrix and conduit, and δ_m for external sources. Although the cross-sectional area parameter A_c shown in Figure 2, we have reduced the dimensionality of the conduit to 1D using a homogenization strategy described by [5]. We are therefore dealing with a coupled 3D/1D flow system. The system described by equation (1) is completed by the boundary conditions $p_m = g_D$ on the left and right sides and $\mathbf{u}_m \cdot \mathbf{n} = 0$ on the other boundaries of Ω, where g_D represents an imposed pressure and $\mathbf{n}$ is the unitary normal pointing outwards to Ω.

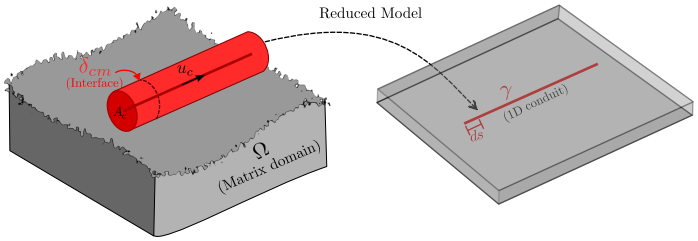

Figure 1: Sketch of the lower dimensional model reduction of a karst conduit. Source: Authors.

We have discretized the domain with a uniform Cartesian grid, as shown in Figure 2. Triangular markers denote flux unknowns within Ω and on its boundary $\partial\Omega$, while circles represent flux unknowns along γ. The karst subdomain was discretized separately and integrated into the matrix grid to ensure geometric stability and alignment.

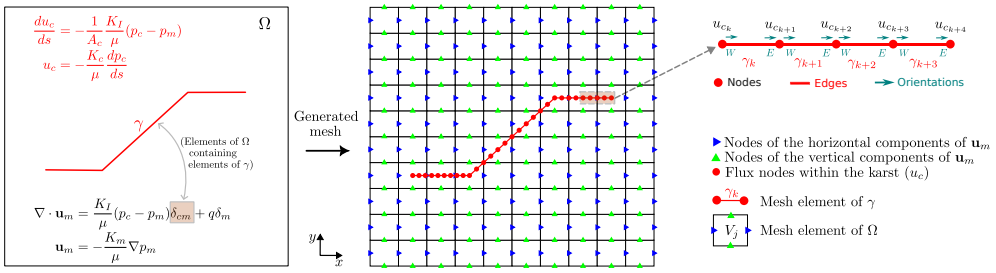

Figure 2: Illustration of the discretized section of a 2D square domain. Source: Authors.

Based on the classical formulation of finite volume methods, the porous matrix equations of system (1) were integrated over each volume element V_j of Ω. Equations associated with conduit elements γ_k of the γ domain were discretized considering the three highlighted feature groups, as shown in Figure 2. We associate the approximated divergence operator with the pressure unknowns within the karst (edges). Flux equations are treated at the nodes, where the conservation condition is imposed. This conservation is formulated by considering an intermediate pressure p_h that acts as a Lagrange multiplier. The semi-discretized equations are arranged as follows:

$$\int_{\partial V_j} \mathbf{u}_{m_j} \cdot \mathbf{n}\, d\partial V_j = \frac{K_I}{\mu}(p_{c_k} - p_{m_j})|_{\gamma_k \cap V_j} + q(\mathbf{x}_j) \qquad \text{(Mass conservation in } \Omega\text{)}, \quad (2)$$

$$\int_{V_j} \mathbf{u}_{m_j}\, dV_j = -\int_{V_j} \frac{K_{eff}}{\mu} \nabla p_{m_j}\, dV_j \qquad \text{(Darcy's law in } \Omega\text{)}, \quad (3)$$

$$\int_{\gamma_k} \frac{du_{c_k}}{ds_k}\, d\gamma_k = -\frac{1}{A_{c_k}} \int_{\gamma_k} \frac{K_I}{\mu}(p_{c_k} - p_{m_j})\, d\gamma_k \qquad \text{(Divergent equation in } \gamma\text{)}, \quad (4)$$

$$\int_{\gamma_k} u_{c_k}^W\, d\gamma_k - \int_{\gamma_k} u_{c_k}^E\, d\gamma_k = 0 \qquad \text{(Mass conservation in } \gamma\text{)}, \quad (5)$$

$$\int_{\gamma_k} \tilde{u}_{c_k}\, d\gamma_k + \int_{\gamma_k} \frac{K_{c_k}}{\mu} \frac{dp_{c_k}}{ds_k}\, d\gamma_k = 0, \quad \tilde{u}_{c_k} \in \{u_{c_k}^W, u_{c_k}^E\} \qquad \text{(Darcy's law in } \gamma\text{)}. \quad (6)$$

In equation (2), $q(\mathbf{x}_j) \neq 0$ if $\mathbf{x}_j \in V_j$ is a location that represents a point source; in equation (3), K_{eff} is the harmonic-mean permeability between the values in V_j and the adjacency V_{j_α}; in equation (5), $u_{c_k}^W$ and $u_{c_k}^E$ are the average flux at nodes (see Figure 2). After the integration process and the ordering of the terms, we obtain a linear system with the following matrix configuration:

$$\begin{bmatrix} \mathbf{M}_{mc} & \mathbf{D}_m & \mathbf{M}_{cm} & \mathbf{0} & \mathbf{0} \\ \mathbf{G}_m & \mathcal{H}_m & \mathbf{0} & \mathbf{0} & \mathbf{0} \\ \mathcal{M}_{mc} & \mathbf{0} & \mathcal{M}_{cm} & \mathbf{0} & \mathbf{D}_c \\ \mathbf{0} & \mathbf{0} & \mathbf{0} & \mathbf{0} & \mathcal{D}_c \\ \mathbf{B}_c & \mathbf{0} & \mathbf{N}_c & \mathbf{N}_h & \mathcal{H}_c \end{bmatrix} \begin{bmatrix} \mathbf{p}_m \\ \mathbf{u}_m \\ \mathbf{p}_c \\ \mathbf{p}_h \\ \mathbf{u}_c \end{bmatrix} = \begin{bmatrix} \mathbf{q}_m \\ \mathbf{0} \\ \mathbf{0} \\ \mathbf{0} \\ \mathbf{0} \end{bmatrix}, \quad (7)$$

where $\mathbf{M}_{mc}$, $\mathbf{M}_{cm}$, $\mathcal{M}_{mc}$ and $\mathcal{M}_{cm}$ are the coupling matrices between Ω and γ; $\mathbf{D}_m$ and $\mathbf{D}_c$ are the discretized divergence operators for matrix and conduit; $\mathbf{G}_m$ is the discretized gradient operator for matrix; $\mathcal{H}_m$ and $\mathcal{H}_c$ are coefficients of the Darcy's law that generate velocity connections for

DOI: 10.5540/03.2026.012.01.0299

matrix and conduit; $\mathcal{D}_c$ is the block responsible for imposing the difference between fluxes at the same node of the conduit to ensure mass conservation; $\mathbf{B_c}$ is the block that set the pressure at the ends of the conduit; $\mathbf{N_c}$ and $\mathbf{N}_h$ have the function of performing a gradient operation between $p_c(s_k)$ and $p_h(s_{k\pm1/2})$; $\mathbf{p}_m$, $\mathbf{p}_c$ and $\mathbf{p}_h$ are the matrix, conduit and intermediate pressure vectors, respectively; $\mathbf{u}_m$ is the vector of velocities components in the matrix and $\mathbf{u}_c$ the vectors of average fluxes in the conduit; $\mathbf{q}_m$ is the source term for the matrix that we will consider null vector. Since the values of the unknowns related to the karst depend on the unknowns associated with the rock matrix, we consider boundary conditions where the pressure on this ends is equal to the pressures of the matrix cells containing the ends of the karst.

Finally, to complete the Finite Volume Karst Flow formulation (denoted FVKF), K_I is calculated as follows:

$$K_I = \frac{2A_L}{(L_m/K_m) + (L_c/K_c)}, \tag{8}$$

where A_L is the contact area open to flow, L_i is the block length, and K_i is the permeability, $i \in \{c, m\}$ [1].

3 Numerical Experiments

In the following simulations we consider the domain $\Omega = 1.0\,\text{m} \times 1.0\,\text{m} \times 0.1\,\text{m}$, permeabilities $K_c = 3.38 \times 10^{-7}\,\text{m}^2$ and $K_m = 3.38 \times 10^{-12}\,\text{m}^2$, as adopted by [8], constant radius $r_c = 10^{-3}\,\text{m}$ for the conduit, and dynamic viscosity $\mu = 8.9 \times 10^{-4}\,\text{Pa.s}$. We also set imposed $g_D = 100\,\text{Pa}$ at the left boundary and $g_D = -100\,\text{Pa}$ at the right boundary.

As a reference solution for comparing the behavior of our results, we use a FEniCSx code [6] for modeling a tridimensional domain containing a high-permeability cylindrical shape at a very refined grid. In this more realistic approach, Darcy's law models the fluid flow in the entire domain (porous matrix and conduit), $\Omega_T = \Omega \cup \gamma$, and leads to the variational finite element problem that can be find in [2]. We also introduce the discrete Raviart-Thomas (RT) subspaces with degree 1 to ensure the velocity has continuos normal component. This spaces are used in combination with the Discontinuos Galerkin (DG) with degree 0 as the space of functions for pressure field.

The results of our numerical experiments are shown in Figures 3-7, where we compare results obtained by the FVKF formulation and the FEniCSx reference solution. Two configurations are studied: a horizontal conduit case and an oblique conduit case.

Resulting slices produced considering a horizontal conduit that has ends at geometric positions (0.25, 0.55, 0.05) and (0.75, 0.55, 0.05) are shown in Figure 3. The permeability field and discretized tridimensional FEniCSx domain illustrated in Figure 3 (left) exhibit the permeability contrast of order 10^5 between the conduit and matrix. To capture the cylindrical region of highest permeability in the reference solution, we impose a higher degree of refinement on the region containing the conduit. The constructed unstructured mesh has 133817 elements. In turn, to apply the finite volume formulation, the matrix domain was discretized with a structured and uniform mesh with $90 \times 90 \times 1$ computational cells, while the conduit domain considers a discretization with 44 elements. Therefore, a total of 8144 elements compose the final FVKF discretized domain, that contains over than 16 times fewer cells than the reference FEniCSx.

The resulting velocity fields yielded by FEniCSx and the FVKF formulation are presented in Figure 3 (center) and (right). It is observed that the flow behavior obtained by the finite volume formulation reproduces with good fidelity the situation taken as reference. Furthermore, the total flux calculated over the domain boundaries produced a result of the order of 10^{-15}, which infers that the mass conservation mass was satisfied.

In the oblique case, with a similar development, we consider the conduit with ends in the geometric positions (0.25, 0.25, 0.05) and (0.75, 0.75, 0.05), that is, a diagonal direction. Figure

DOI: 10.5540/03.2026.012.01.0299

4 shows the slices produced, where the permeability field (left) remains with the same contrast of order 10^5 between conduit and matrix. The discretized tridimensional FEniCSx domain considers an unstructured mesh with 131497 elements, while the finite volume domain considers the same matrix discretization with with $90 \times 90 \times 1$ cells, and the conduit domain with 45 elements. Again, the FVKF discretized domain contains about 16 times fewer cells than the reference FEniCSx.

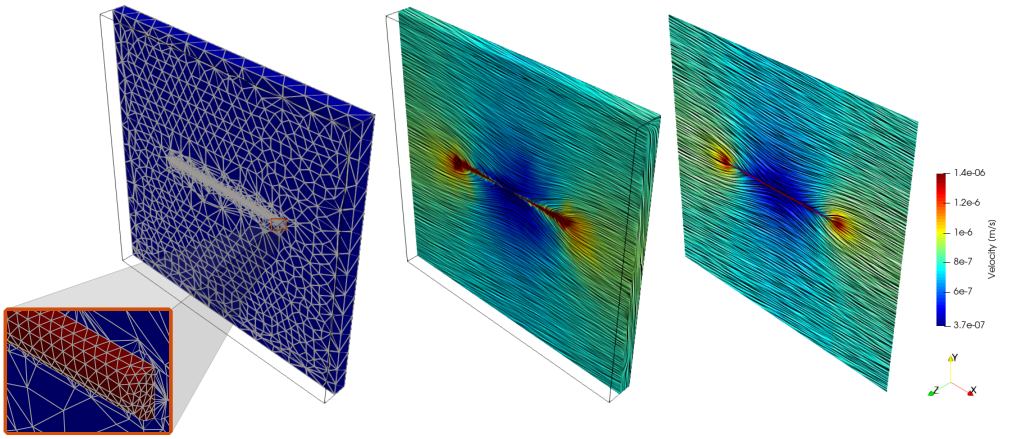

Figure 3: Permeability field and discretized domain in FEniCSx for the horizontal conduit (left); Velocity field obtained by FEniCSx (center); Velocity field obtained by FVKF (right). Source: Authors.

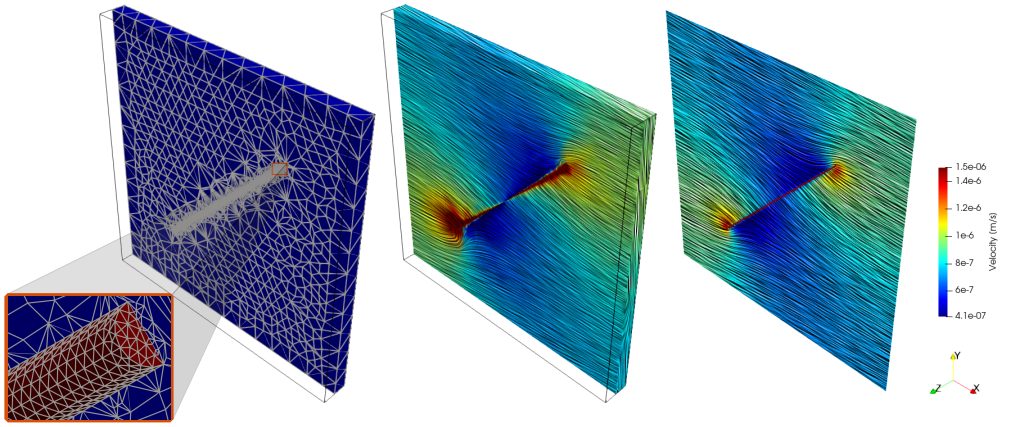

Figure 4: Permeability field and discretized domain in FEniCSx for the oblique conduit (left); Velocity field obtained by FEniCSx (center); Velocity field obtained by FVKF (right). Source: Authors.

Once again, the flow behavior was captured with clear perception by the FVKF formulation, which in addition, also presented mass conservation error in the order of 10^{-15}. The levels of permeability contrast for such binary fields are dominant when compared to cases with intermediate values [9]. Thus, it is expected that FVKF works well for heterogeneous background permeability.

Respective pressure fields are shown in Figure 5, corroborating the good representation yielded by FVKF when capturing the effects generated by the presence of the high permeability channel. This conclusion is further reinforced by the curves shown in Figure 6, in which the pressure drop that occurs at the ends of the channels is also well reproduced by the finite volume formulation.

DOI: 10.5540/03.2026.012.01.0299

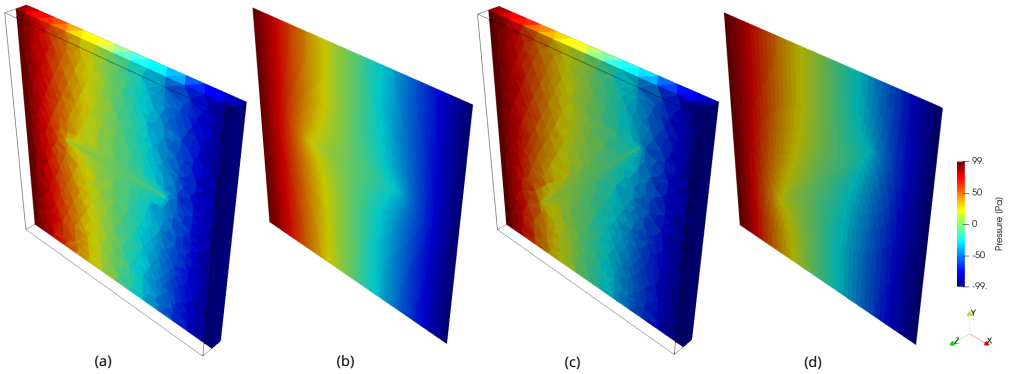

Figure 5: Pressure field for the horizontal conduit obtained by (a) FEniCSx and (b) FVKF; Pressure field for the oblique conduit obtained by (c) FEniCSx and (d) FVKF. Source: Authors.

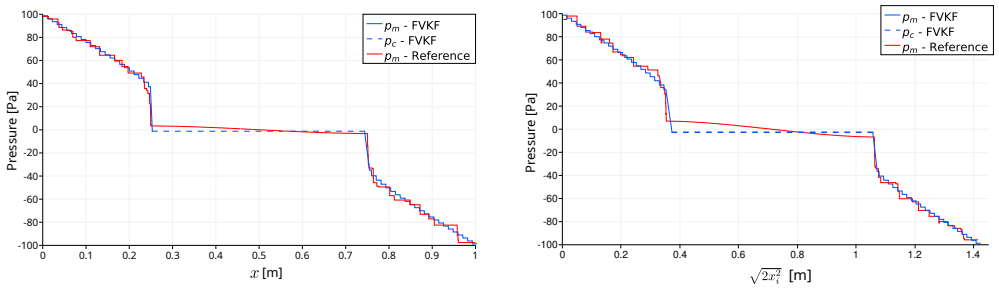

Figure 6: Pressure for the horizontal conduit (left), and for the oblique conduit (right). Source: Authors.

Finally, Figure 7 shows a continuous exchange of mass between the porous matrix and the conduit through the interface that covers the lateral surface of the cylindrical region. These curves were generated by applying the FVKF formulation. It is worth noting that the order of the values for exchanges recorded (10^{-4}), as well as, the order of the indices calculated by equation (8) (10^{-12}) are consistent with the values obtained in [3, 5, 8].

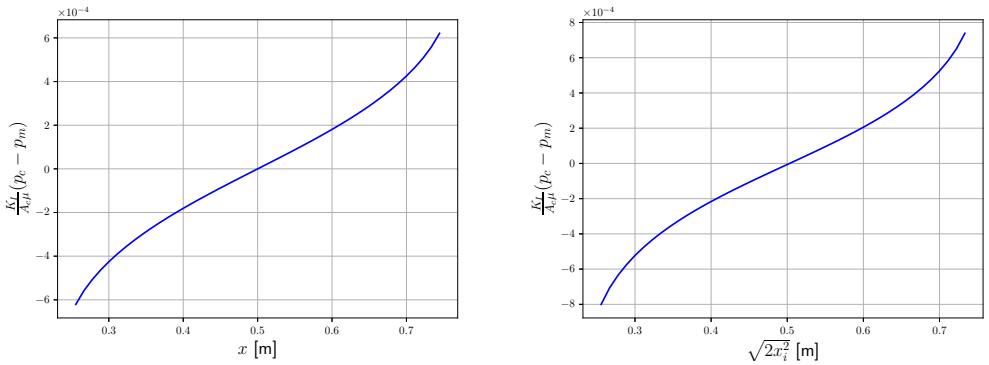

Figure 7: Mass exchange: matrix and horizontal conduit (left); matrix and oblique conduit (right). Source: Authors.

4 Conclusions

With the experiments carried out, the flow behavior in both horizontal and oblique conduits cases could be effectively represented. The structured and unstructured mesh approaches exhibited excellent mass conservation, indicating that the solutions are reliable. In particular, the pressure fields generated by the FVKF formulation closely match the expected pressure drops, which is a further indication of the accuracy of the model. Moreover, the mass exchange analysis confirms a consistent interaction between matrix and conduit, being the values consistent with the literature. These results highlight the ability of the FVKF formulation to provide a good representation of flow in karstified systems and it will be tested on more complex geometries in future work.

Acknowledgements

We acknowledge the financial support from CAPES (Code 001).

References

[1] M. G. Correia, J. C. von Hohendorff Filho, and D. J. Schiozer. "Multiscale Integration for Karst-Reservoir Flow-Simulation Models". In: **SPE Reservoir Evaluation & Engineering** 23.02 (2020), pp. 518–533.

[2] A. Dudun and Y. Feng. "Modeling fluid flow in fractured porous media: a comparative analysis between Darcy-Darcy model and Stokes-Brinkman model". In: **J Petrol Explor Prod Technol** 14 (2024), pp. 909–926.

[3] P. Ferraz, P. Pereira, E. Abreu, and M. A. Murad. "Recursive Mixed Multiscale Model Reduction for Karst Conduit-Flow in Carbonate Reservoirs". In: **Transport in Porous Media** 139 (2021), pp. 527–558.

[4] I. Gjerde, K. Kumar, and J. Nordbotten. "A singularity removal method for coupled 1d–3d flow models". In: **Computational Geosciences** 24 (2020), pp. 443–457.

[5] I. Landim, M. A. Murad, P. Pereira, and E. Abreu. "A new computational model for karst conduit flow in carbonate reservoirs including dissolution-collapse breccias". In: **Computational Geosciences** 27 (2023), pp. 879–912.

[6] H. P. Langtangen and A. Logg. **Solving PDEs in Python The FEniCS Tutorial I**. Springer Nature, 2017.

[7] U. G. Moreira, F. F. Rocha, A. Jaramillo, F. S. Sousa, R. F. Ausas, G. C. Buscaglia, and F. Pereira. "Numerical solution of single-phase flows in karstified heterogeneous carbonate rocks". In: **Proceedings of the XLIII CILAMCE, ABMEC** (2022), pp. 1–66.

[8] M. A. Murad, T. V. Lopes, P. A. Pereira, F. H. R. Bezerra, and A. C. Rocha. "A three-scale index for flow in karst conduits in carbonate rocks". In: **Advances in Water Resources** 141 (2020), pp. 103613.

[9] F. F. Rocha, F. S. Sousa, R. F. Ausas, F. Pereira, and G. C. Buscaglia. "Interface spaces based on physics for multiscale mixed methods applied to flows in fractured-like porous media". In: **Computer Methods in Applied Mechanics and Engineering** 385 (2021), pp. 114035.

[10] C. Wolfsteiner, L. J. Durlofsky, and K. Aziz. "Calculation of well index for nonconventional wells on arbitrary grids". In: **Computational Geosciences** 7.1 (2003), pp. 61–82.

[11] Y. S. Wu. **Multiphase Fluid Flow in Porous and Fractured Reservoirs**. 1st ed. Gulf Professional Pub., 2016.

